

Localization properties of vibrational modes in $a\text{-Si}_3\text{N}_4$

Luigi Giacomazzi^{1,2}

¹ SISSA, Scuola Internazionale Superiore di Studi Avanzati, via Bonomea 265, I-34136 Trieste, Italy.

² Materials Research Laboratory, University of Nova Gorica, Vipavska 11c 5270-Ajdovščina, Slovenia.

E-mail: giacomaz@sissa.it

Abstract. We present a first-principles investigation of the localization properties of vibrational modes in amorphous silicon nitride ($a\text{-Si}_3\text{N}_4$). Our investigation further confirms that the vibrational modes underlaying the peak at $\sim 471\text{ cm}^{-1}$ in the infrared spectrum of silicon nitride mainly consist of nitrogen motion in the direction normal to the nearest Si neighbors plane. In-plane stretching of N–Si bonds becomes largely dominant above $\sim 700\text{ cm}^{-1}$. In particular vibrational modes underlaying the infrared peak at 825 cm^{-1} arise from Si–N bonds stretching motions. If N–N homopolar bonds were present, we show that N–N bond stretching occur above $\sim 1100\text{ cm}^{-1}$. Furthermore, we investigate the localization properties of vibrational modes by calculating their inverse participation ratio (IPR) and phase quotient. From this analysis we infer that modes above 600 cm^{-1} shows a progressive increase of the localization degree and optic-like behavior, especially above 1000 cm^{-1} . At about 650 cm^{-1} , given the considerable IPR value, and on the basis of projectional analysis on silicon-breathing-like motions of the NSi_3 units, we suggest that vibrational modes may involve correlated motions of neighboring SiN_4 tetrahedra.

PACS numbers: 63.50.+x, 78.30.-j, 61.43.Fs, 71.15.Mb

1. Introduction

Nowadays amorphous silicon nitride ($a\text{-Si}_3\text{N}_4$) is widely used in microelectronics e.g. to fabricate insulating layers in triple oxide-nitride-oxide structures [1]. In particular, because of its high concentration of charge traps, $a\text{-Si}_3\text{N}_4$ is employed as charge storage layer in nonvolatile memory devices [2, 3]. Thin films of $a\text{-Si}_3\text{N}_4$ are grown either through chemical vapor deposition [4] (CVD) of silane and ammonia gases or through physical vapor deposition (PVD) [5]. Infrared spectroscopy can then be adopted for characterizing films composition and stoichiometry [6]. For instance, the intensity of infrared absorption peaks around 2220 and 3300 cm^{-1} , arising from Si–H and N–H stretching modes respectively, can be used to estimate the hydrogen content [7, 8, 9].

The experimental infrared dielectric function of $a\text{-Si}_3\text{N}_4$ features two main broad peaks at 471 cm^{-1} and 825 cm^{-1} [10, 11]. These peaks are then slightly shifted in the absorption spectrum where they appear respectively at about 490 cm^{-1} and 900 cm^{-1} [10]. The former peak was attributed to silicon-breathing motion [7, 12], meanwhile the latter high frequency peak at 900 cm^{-1} is commonly assigned to Si–N

bond stretching [7, 13]. The assignement of the 490 cm^{-1} feature [7] invoked a breaking of symmetry caused by the presence of hydrogen atoms. However as shown in Ref. [14] the presence of hydrogen seems not very relevant for explaining this feature, that instead appear to be originated by out-of-plane nitrogen motion. In Ref. [15] a feature at about 640 cm^{-1} was observed in the absorption spectrum of silicon nitride films. In particular in Ref. [15] it is shown that this feature is not affected by hydrogen content and thus can not be related to Si–H stretching modes. By invoking an analogy to the absorption bands in $a\text{-SiO}_2$, this feature at 640 cm^{-1} was tentatively assigned to some unspecified vibration of the NSi_3 unit [15]. Moreover it has been proposed that a feature appearing at 644 cm^{-1} could be originated by silicon-breathing-like motions of the NSi_3 unit [10]. Incidentally we note that such an hypothesis suggests implicitly a larger localization degree of the vibrational modes with respect to the typical localization of modes in glasses up to a few hundred cm^{-1} . On the other hand, in recent years the vibrations in the medium frequency range (520 to 770 cm^{-1}) were further ascribed, for the $\alpha\text{-Si}_3\text{N}_4$ crystalline phase, to vibrations of Si atoms in SiN_4 tetrahedra [29, 30].

On the theoretical side, density functional approaches have successfully complemented and helped to interpret experimental spectroscopic data, thereby considerably enriching the knowledge of the network organization and ions dynamics in several materials e.g. v- SiO_2 [16, 17, 18], v- GeSe_2 [20, 21], v- B_2O_3 [22]. Despite in the recent years several theoretical works have investigated the structural and electronic structure properties of systems based on silicon nitride [23, 24, 26, 27, 28], only a few of them have discussed the vibrational properties [29, 31].

In this paper, we discuss the origin of vibrational bands in silicon nitride by comparing the vibrational spectra of two first-principles model structures of amorphous silicon nitride. The first of these two models was generated in Ref. [14] and contains a small amount of hydrogen atoms ($\sim 0.1\%$ wt). A second smaller model, hydrogen free, is generated in this work with the aim of strengthening our analysis by exploiting comparisons among structurally different models, by ruling out any hypothetical relevant effect due to the hydrogen presence on the v-DOS in the medium frequency range, and finally by allowing to discuss specific vibrations of N–N homopolar bonds which are absent in our first model [14]. The vibrational density of states are first analysed by means of decomposition into N and Si contributions. Then, silicon nitride vibrational modes are analysed in terms of vibrations of the N–N and NSi_3 units. Finally we investigate the nature of vibrational modes by examining their localization properties through the inverse participation ratio (IPR) and phase quotient [32]. The present analysis aims at giving a general description of the vibrational modes of $a\text{-Si}_3\text{N}_4$ with a special attention to those around $\sim 650\text{ cm}^{-1}$, at the crossover between the two main absorption bands. Moreover, this investigation further discusses the assignment of the peak at 490 cm^{-1} in the infrared absorption spectrum to vibrational modes featuring nitrogen motion in direction normal to the silicon neighbors plane [33, 14], by considering analysis on multiple models.

The paper is organised as follows. In Sec. 2, we concisely describe the methods adopted in the present work. We also outline how we generated our model structures as well as their main structural features. In Sec. 3, we analyse the vibrational density of states and the localization aspects of the vibrational modes of our models. Furthermore, we discuss the infrared spectra of our models in comparison with experimental results. We draw conclusions in Sec. 4.

2. Methods and models

2.1. Methods

In the present work, we have performed first-principles electronic-structure calculations based on density functional theory. For generating the model structures of $a\text{-Si}_3\text{N}_4$ we carried out molecular dynamics simulations using the Car-Parrinello method [34, 35]. In particular, we used the computational codes and pseudopotentials from the QUANTUM-ESPRESSO package [36]. The exchange and correlation functional was approximated through the local density approximation (LDA) [37]. Core-valence interactions were described through ultrasoft pseudopotentials [38] for N and through a normconserving pseudopotential for Si atoms. The electronic wavefunctions and the charge density were expanded using plane waves basis sets defined by energy cutoffs of 25 Ry and 200 Ry, respectively. The Brillouin zone was sampled at the Γ point. We derived the vibrational frequencies and eigenmodes by diagonalizing the dynamical matrix, [16] which we calculated numerically by taking finite differences of the atomic forces. To this purpose we used atomic displacements of 0.05 Bohr. In Ref. [14] we obtained the relevant coupling tensors needed to calculate infrared spectra by taking advantage of a scheme for applying a finite electric field in periodic cell calculations [39, 16]. An alternative way for calculating the coupling tensors i.e the dynamical charges is to perform linear-response calculations [40] as implemented in the QUANTUM-ESPRESSO package [36]. In this work we obtained the dynamical charges of the model labelled as Model II (see 2.2) by following the latter approach.

2.2. Model generation procedure

In this work we consider two models of silicon nitride. The first one was generated by first-principles molecular dynamics [14] through a quench-from-the-melt approach, as described here above. This model has a size of 152 atoms in a simulation cell of 22.1 bohr. In the following we will refer to this model as Model I. A smaller model with a size of 70 atoms (Model II) was here generated starting from a supercell of $\beta\text{-Si}_3\text{N}_4$ that was rescaled to match the experimental value of the density 3.1 g/cm³ [41, 42]. Molecular dynamics runs were then performed for obtaining the model of $a\text{-Si}_3\text{N}_4$. First the system was thermalized at the temperature of 3700 K for 12 ps using a Nosé-Hoover thermostat [43]. Successively, the sample was quenched for 7 ps down to 1600 K below the theoretical melting point. Finally, the structural geometry was further optimized by a damped molecular-dynamics run.

2.3. Structural properties

In Tab. 1 we summarize the main structural parameters of our models. Both Model I and II show an average Si–N bond length of about 1.73 Å with a similar standard deviation of ~ 0.06 Å. The average Si–N–Si and N–Si–N bond angles are 117° and 109° as typical for silicon nitride models [44, 45]. The calculated radial distribution function of Model II [Fig. 1] is very similar to that found for Model I [14] and in fair agreement with the experimental results [46], thus assuring that also Model II provides a fair structural description of silicon nitride. In Model II we register the presence of ten two-fold rings, while in Model I we found sixteen [14]. 47% of silicon atoms in Model II belong to such rings, slightly more than in Model I where we register 39% [14]. A few under- and over-coordinated nitrogen and silicon atoms are also found. Moreover the

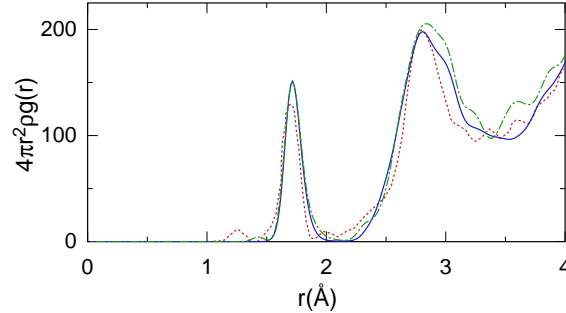


Figure 1. Radial distribution function of *a*-Si₃N₄ calculated at room temperature for Model I (solid/blue), Model II (dot-dashed/green) and experimental data from Ref. [46] (dotted/red).

Table 1. Structural parameters of our models of *a*-Si₃N₄. N is the number of atoms in the simulation cell. d_{SiN} indicates the bond length and is given in Å. Si-N-Si corresponds to the average intertetrahedral angle. Standard deviations are given in parenthesis. Experimental d_{SiN} is taken from Ref. [46] and values referring to Model I are taken from Ref. [14].

	N	d_{SiN}	N-Si-N	Si-N-Si
Model I	152	1.73 (0.06)	109.1° (13°)	117.2° (15.1°)
Model II	70	1.74 (0.07)	108.9° (13.4°)	117.0° (15.9°)
Expt.		1.729		

structure contains a N–N homopolar bond with a bond length of 1.4 Å. This is rather close to the value (\sim 1.2 Å) reported e.g. for the N–N bond length in a first-principle investigation of the liquid phase [47] and is 0.2 Å shorter than the value found in [25] for a nonstoichiometric system Si₃N_{4.5}. We note however that the concentration of such type of bonds in *a*-Si₃N₄ is rather controversial [25, 48, 49] and investigating this issue goes beyond the scope of the present work. Despite the presence of point defects as mentioned above, in both Model I and II most (\sim 90%) of nitrogen and silicon atoms are three- and four-fold coordinated [14].

3. Vibrational density of states

3.1. Nitrogen out-of-plane and stretching motions

In Fig. 2 we compare the v-DOS of the two models of *a*-Si₃N₄. The v-DOS of the two models are quite similar with a pronounced peak at about 400 cm⁻¹ and broad bands extending up to about 1250 cm⁻¹. Next, in Fig. 2(c), we show the imaginary part of the dielectric function of Model I and II. Both models show infrared spectra of similar fair quality when compared to the infrared spectrum obtained from experiments [11]. Minor differences between the two spectra of Model I and II are noticeable especially in the central frequency region from about \sim 500 cm⁻¹ up to 900 cm⁻¹. These minor differences should be attributed to small structural differences (Fig. 1) between the two models as well as to size effects and are quite typical in modelling glassy materials [19, 20, 16].

The decomposition of the v-DOS shown in Fig. 2(a) for Model I, in terms of silicon and nitrogen and hydrogen weights is essentially the same as that shown in Fig. 2(b) for the v-DOS of Model II, thus further supporting the reasonable assumption that a low concentration of hydrogen will provide only a negligible contribution to the v-DOS below $\sim 1000 \text{ cm}^{-1}$ and thus that Model I is perfectly suitable to discuss the vibrational properties also of pure Si_3N_4 glass. In both models the nitrogen contribution to the v-DOS features a two humps camel shape with broad maxima at about 400 and 900 cm^{-1} , while the silicon contribution has broad maxima at about 350 and 650 cm^{-1} . Despite in Fig. 2(a) the peak at 650 cm^{-1} of the silicon contribution is more pronounced than the corresponding one in Fig. 2(b), we note that for both models we can easily identify such a feature. We thus conclude that this peak at about 650 cm^{-1} in the v-DOS does constitute a distinctive feature of the v-DOS of glassy silicon nitride as well as of the crystalline phase $\alpha\text{-Si}_3\text{N}_4$ where the crystal symmetries appear to enhance it [29]. By contrast, we note that such a feature is absent in the v-DOS obtained by using force fields for models generated by classical molecular dynamics [45, 54, 53]. Classical modeling approaches are generally not sufficiently accurate [51, 52] for describing vibrational properties of vitreous silica, thus we suggest that classical force fields also fail in describing silicon nitride vibrational modes around 650 cm^{-1} .

In Fig. 3(a) we decompose the nitrogen contribution to the v-DOS of Model II according to three orthogonal directions defining the local environment of the N atoms as we have previously done for Model I [14]. The first direction, which we refer to as out-of-plane or rocking, is taken orthogonal to the plane of the three nearest Si neighbors. Then, the second one is taken along the bisector of one of the three Si-Si-Si angles and the third one is given by the cross product of the first two. The latter two directions define the stretching motion in the plane of the three nearest Si neighbors. This decomposition in terms of rocking and stretching motions allow to establish the existence of two separate nitrogen bands below and above $\sim 600 \text{ cm}^{-1}$. Fig. 3(a) further supports the result of Ref. [14] i.e. the contribution to the nitrogen partial v-DOS due to out-of-plane motions is maximised at about 350 to 450 cm^{-1} , while the contribution due to stretching motions accounts for almost all the nitrogen v-DOS above $\sim 700 \text{ cm}^{-1}$.

3.2. Projection on NSi_3 silicon-breathing and N-N stretching modes

Infrared spectra of amorphous silicon nitride show a small, yet non-negligible intensity between the two main peaks at 471 and 825 cm^{-1} . In Ref. [10, 15] it was proposed that modes belonging to this central region, and in particular a fitted absorption band at $\sim 640 \text{ cm}^{-1}$, could be interpreted in terms of some vibration of the NSi_3 unit, eventually in terms of the silicon-breathing mode [Fig. 3(b)]. For symmetry reasons this mode of the NSi_3 unit is Raman active but not infrared active [7]. However the ideal symmetry shown in the mode depicted in Fig. 3(b) is not necessarily respected in the silicon nitride network where NSi_3 units may have a distorted geometry. As soon as the symmetry is broken the silicon-breathing mode can become infrared active [7]. Moreover from Figs. 2 and 3 we remark that at about 650 cm^{-1} nitrogen displacements do stretch N-Si bonds, so that in general we do not have just silicon displacements as in the very ideal case of Fig. 3(b), but more in general vibrational modes will involve several SiN_4 tetrahedra, and hence a considerable nitrogen motion. Still, it is interesting to investigate what type of silicon motion may take place in the

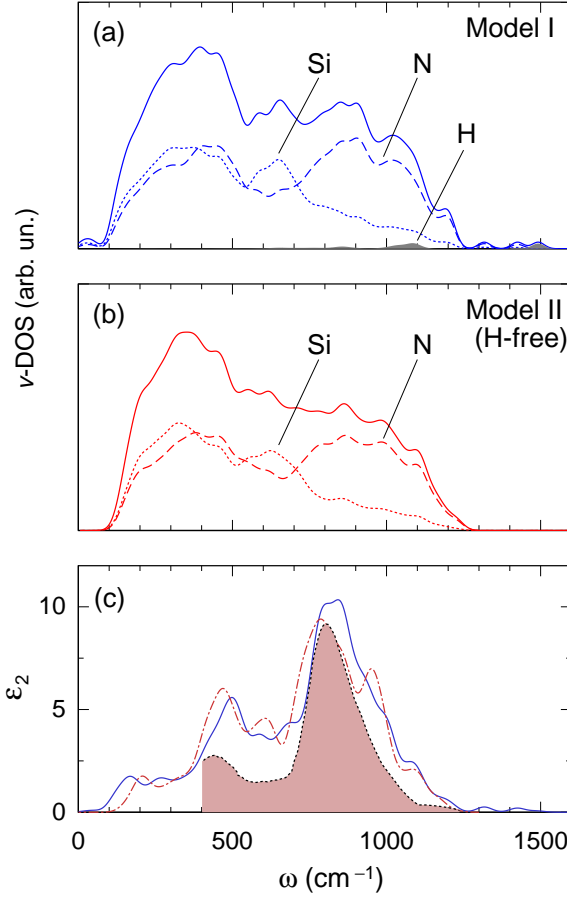


Figure 2. v-DOS (solid) and silicon (dotted) and nitrogen (dashed) contribution to the density of states for (a) Model I [Ref. [14]] and (b) Model II. (c) Calculated imaginary part of the dielectric function (ϵ_2) for Model I (solid/blue) and for Model II (dot-dashed/red) and experimental results (dotted/shaded pink) of Ref. [11]. A Gaussian broadening of 25 cm^{-1} was applied.

frequency range between the two main peaks of the infrared dielectric function and if the projection on some NSi_3 unit mode can be of help to understand some property of the vibrational modes in the region 500 to 700 cm^{-1} . By considering the vibrational modes of our model structures we investigate the frequency localization of silicon-breathing motions in amorphous silicon nitride. First, we project the vibrational eigenmodes onto the ideal silicon-breathing mode [Fig. 3(b)] for each NSi_3 unit. Next by calculating the average of these projections we obtain the average weight of silicon-breathing motions as function of the frequency [19]. The result shown in Fig. 3(b) indicates the presence of just one broad peak at about 650 cm^{-1} in both in Model I and Model II and with a width at half maximum of about two hundreds of cm^{-1} . Furthermore, we explicitly count all the NSi_3 units showing silicon motion compatible with the ideal silicon-breathing mode. In the frequency range between 620 and 680 cm^{-1} silicon-breathing-like motions involve up to 20% of the NSi_3 units. The result of

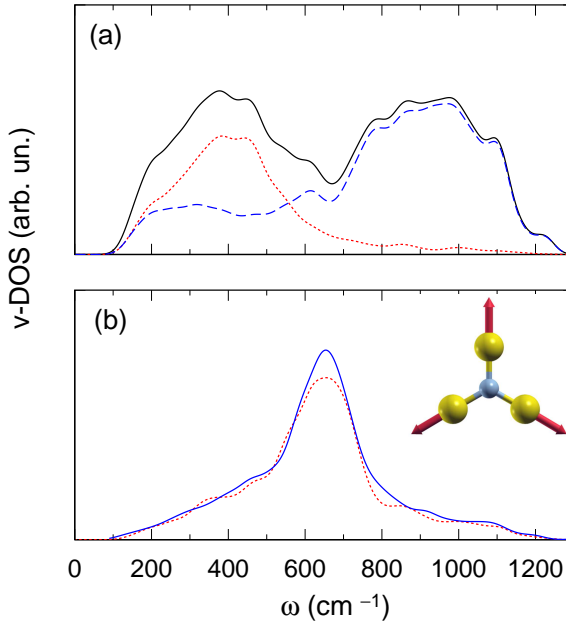


Figure 3. (a) Decomposition of the nitrogen contribution (solid) to the v-DOS of Model II into motions along the normal to the plane of silicon neighbors (dotted/red) and into stretching motions in the plane of silicon neighbors (dashed/blue). Only threefold coordinated nitrogen atoms are taken into account. (b) Average projections of the vibrational eigenmodes onto silicon-breathing motions for Model I (solid/blue) and Model II (dotted/red). A Gaussian broadening of 25 cm $^{-1}$ was applied.

Fig. 3(b) indicates the presence of correlated motions involving a few SiN_4 neighboring tetrahedra which at about 650 cm $^{-1}$ has an important component on the NSi_3 plane. By comparing with Fig. 2(b) we infer that such type of correlated motion is almost absent below ~ 400 cm $^{-1}$. On the other hand above ~ 750 cm $^{-1}$ nitrogen stretching, involving a higher localization degree as discussed hereafter [50], appear to dominate the v-DOS, while Si contribution to the v-DOS fades away [Fig. 2].

In Fig. 4 we show the vibrational density of states obtained by projecting the vibrational eigenmodes on the nitrogen-nitrogen stretching motion of the N–N homopolar bond present only in Model II. The projection shows a sharp peak at about ~ 1150 cm $^{-1}$. We remark that shorter N–N bonds [48, 47] should give rise to higher frequencies peaks as it is the case for instance of two-fold coordinated nitrogen atoms [14], and viceversa longer N–N bonds will show lower stretching frequencies. We thus infer that stretching of N–N homopolar bonds should only affect the high frequency tail (above ~ 1100 cm $^{-1}$) of the infrared dielectric function shown in Fig. 2(c).

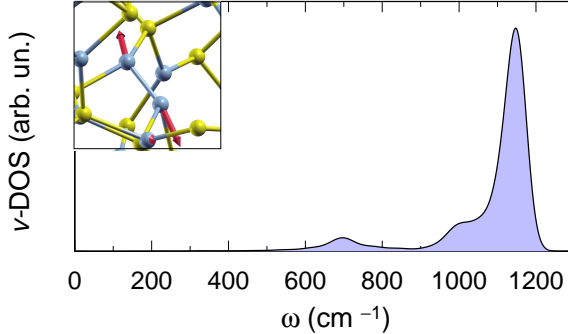


Figure 4. Projection of the vibrational eigenmodes of Model II onto nitrogen-nitrogen stretching motion. In the inset a snapshot of a vibrational mode at 1160 cm^{-1} is shown. A Gaussian broadening of 25 cm^{-1} was applied.

3.3. Localization properties of vibrational modes

We investigate the spatial localization of the eigenmodes by calculating the inverse participation ratio (IPR) π_j [32] for the eigenmode j :

$$\pi_j = N \frac{\sum_{i=1}^N |\mathbf{u}_i^j|^4}{(\sum_{i=1}^N |\mathbf{u}_i^j|^2)^2} \quad (1)$$

where N is the number of atoms, and \mathbf{u}_i^j indicates the displacement of the i atom [16]. For an ideally delocalised mode, the IPR is exactly one, and the larger the IPR the more localised the mode is. In Fig. 5(a) we show the IPR of the vibrational modes of our largest model [Model I, Ref. [14]]. We note that modes up to $600\text{--}620\text{ cm}^{-1}$ have a quite low IPR (up to ~ 2) indicating a delocalised nature of these modes. However for vibrational modes with frequencies about $\sim 620\text{ cm}^{-1}$ we observe an IPR of ~ 6 , a few times larger than the one of delocalised modes. Then up to 1050 cm^{-1} IPR shows a slowly increasing trend. Above 1050 cm^{-1} the IPR further increases to values that indicate an even stronger localization degree (IPR ~ 30). Incidentally we note that the upper limit of the delocalised modes ($\sim 600\text{ cm}^{-1}$) actually corresponds to the fading away of the "rocking" modes of the nitrogen [14]. In other words as soon as nitrogen start moving mainly on the Si–N bonds plane, then the vibrational modes become slightly more localised, and in particular the IPR registers a localization peak at about $\sim 650\text{ cm}^{-1}$ in correspondance of the projection peak shown in Fig. 3. The localization then progressively increases and above $\sim 1000\text{ cm}^{-1}$ it shows a jump to ~ 30 indicating localization of a few nitrogen atoms [Fig. 2(a)]. We note that the slow passage from delocalised to localised states that takes place in the frequency window $600\text{--}700\text{ cm}^{-1}$ includes the region of the peak of the silicon partial density of states (Fig. 2) and also the peak of the projection on the silicon breathing mode [Fig. 3(b)].

Besides the IPR another quantity that is useful for analysing the local behavior of the eigenmodes is the phase quotient [32],

$$q_j^{(2)} = \frac{1}{\sum_{i,i'} |\mathbf{e}^j_i|^2} \sum_i \sum_{i'} \frac{\mathbf{u}_i^j \cdot \mathbf{u}_{i'}^j}{|\mathbf{u}_i^j| \cdot |\mathbf{u}_{i'}^j|} |\mathbf{e}^j_i|^2 \quad (2)$$

where \mathbf{u}_i^j indicates the displacement of the i silicon and i' runs over its nearest nitrogen neighbors. j labels the normalised vibrational mode \mathbf{e}^j [16]. The phase quotient

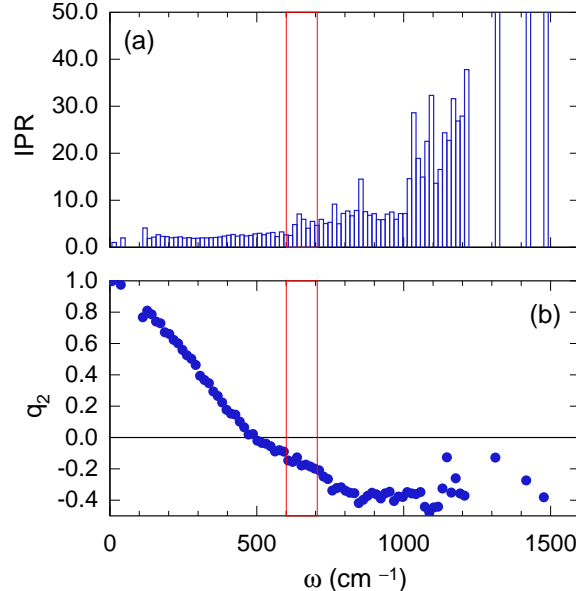


Figure 5. (a) Inverse participation ratio of the vibrational modes of Model I. Values are averaged over an interval of 15 cm^{-1} . (b) Phase quotient of the vibrational modes of the silicon nitride Model I. Values are averaged over an interval of 15 cm^{-1} . Interval $600\text{--}700 \text{ cm}^{-1}$ is emphasized with a pink box.

corresponds, for a given silicon atom, to the average cosinus of the angle between the atomic displacements of its nearest nitrogen neighbors. In Fig. 5(b) we show the phase quotient (q_2) calculated for Model I. Modes at low frequencies show an acoustic-like behavior with neighboring atoms moving in phase ($q_2 \sim 1$). The phase quotient then decreases almost linearly and at about 500 cm^{-1} becomes zero, indicating that nitrogen and silicon atoms have on average orthogonal displacements. Moreover in this region [Fig. 2(a) and (b)] nitrogen rocking motions are dominant. Above $\sim 600 \text{ cm}^{-1}$ modes start to show an optic-like behavior with neighbors moving in anti-phase ($-1 < q_2 < 0$). The phase quotient further decreases in the stretching region above 800 cm^{-1} . The behavior of the phase quotient in silicon nitride appears qualitatively similar to that registered in $v\text{-SiO}_2$ with an almost linear trend up to 800 cm^{-1} where we note a saturation $q_2 \sim -0.4$ corresponding to the Si–N bond stretching modes [32].

4. Conclusion

The present first-principles investigation has focussed on localization aspects of vibrational modes in $a\text{-Si}_3\text{N}_4$ systems. Moreover, the present work provides further support for the interpretation of the 471 cm^{-1} and 825 cm^{-1} peaks of the infrared dielectric function of $a\text{-Si}_3\text{N}_4$ as due to nitrogen motion in the direction normal to the nearest Si neighbors plane and to Si–N bond stretching motion, respectively [14]. From the inverse participation ratio and phase quotient analysis we infer that modes above 600 cm^{-1} show a progressive increase of localization and optic-like behavior with modes that become highly localized above 1000 cm^{-1} . In particular at about 650 cm^{-1} the vibrational modes are considerably more localized than below 600 cm^{-1} .

and, moreover, our analysis based on projection onto silicon-breathing-like modes of the NSi₃ units suggests that correlated motions of a few neighboring SiN₄ tetrahedra can take place at about 650 cm⁻¹, and may sometimes appear as ring modes, at the crossover frequency between the two main bands of the infrared spectrum.

References

- [1] Ma Y, Yasuda T, and Lucovsky G, 1994 *Appl. Phys. Lett.* **64**, 2226
- [2] Aozasa H, Ujiwara I F, Nakamura A and Komatsu Y, 1999 *Jpn. J. Appl. Phys.* **38**, 1441; Bachhofer H, Reisinger H, Bertagnolli E, and von Philipsborn H, 2001 *J. Appl. Phys.* **89**, 2791
- [3] E. Vianello, F. Driussi, P. Palestri, D. Esseni, L. Perniola, G. Molas, and L. Selmi 2011 *IEEE Trans. Elect. Devices* **58**, 2483; 2011 *IEEE Trans. Elect. Devices* **58**, 2490
- [4] Pierson H O, *Handbook of chemical vapor deposition* Noyes Publications (Norwich, New York, 1999).
- [5] Mattox D M, *Handbook of physical vapor deposition (PVD) processing*, Noyes Publications (Westwood, New Jersey, 1998).
- [6] O. Debieu *et al.*, 2013 *Nanoscale Res. Lett.* **8**, 31
- [7] Lucovsky G, Yang J, Chao S.S, Tyler J.E, and Czubatyj W 1983 *Phys. Rev. B* **28**, 3234; Tsu D.V, Lucovsky G, and Mantini M.J, 1986 *Phys. Rev. B* **33**, 7069
- [8] Verlaan V, van der Werf C.H.M. , Arnoldbik W.M., Goldbach H.D., and Schropp R.E.I., 2006 *Phys. Rev. B* **73**, 195333
- [9] Kang-Cheng Lin and Si-Chen Lee, 1992 *J. Appl. Phys.* **72**, 5474
- [10] Tice J B, D'Costa V R, Grzybowski G, Chizmeshya AVG , Tolle J, Menendez J and Kouvettakis J, 2010 *Chemistry of Materials* **22** , 5296
- [11] Gunde M. K. and Maćek M., 2001 *Phys. Stat. Sol. A* **183**, 439
- [12] In molecular systems such as trisilylamine, a mode at 490 cm⁻¹ is assigned to a silicon-breathing vibration [55]. The 471 cm⁻¹ frequency peak of the infrared spectrum of *a*-Si₃N₄ is clearly quite close to the frequency of the silicon-breathing vibration in trisilylamine. However in passing from a molecular system to an extended one some caution should be used and in general there is no strict correspondence between the vibrational modes of an extended system and those of a molecule formed by atoms of the same species.
- [13] Pandey R. K., Patil L. S., Bange J.P, and Gautam D. K., 2004 *Opt. Materials* **27**, 139
- [14] Giacomazzi L and Umari P, 2009 *Phys. Rev. B* **80**, 144201
- [15] Yin Z and Smith F W, 1990 *Phys. Rev. B* **42**, 3666
- [16] Giacomazzi L, Umari P, and Pasquarello A, 2009 *Phys. Rev. B* **79**, 064202
- [17] Pasquarello A and Car R, 1997 *Phys. Rev. Lett.* **79**, 1766
- [18] Pasquarello A and Car R, 1998 *Phys. Rev. Lett.* **80**, 5145
- [19] Giacomazzi L, Umari P, and Pasquarello A, 2006 *Phys. Rev. B* **74**, 155208; Giacomazzi L, Umari P, and Pasquarello A, 2005 *Phys. Rev. Lett.* **95**, 075505
- [20] Giacomazzi L, Massobrio C, and Pasquarello A, 2011 *J. Phys. Cond. Matter* **23**, 295401
- [21] Micoulaut M, Kachmar A, Bauchy M, Le Roux S, Massobrio C, and Boero M, 2013 *Phys. Rev. B* **88**, 054203
- [22] Umari P and Pasquarello A, 2005 *Phys. Rev. Lett.* **95**, 137401
- [23] Pham T.A, Li T, Shankar S, Gygi F, and Galli G, 2011 *Phys. Rev. B* **84**, 045308
- [24] Pham T.A. *et al.*, 2013 *Appl. Phys. Lett.* **102**, 241603
- [25] L. E. Hintzsche, C. M. Fang, T. Watts, M. Marsman, G. Jordan, M.W.P.E. Lamers, A. W. Weeber, and G. Kresse, 2012 *Phys. Rev. B* **86**, 235204
- [26] Hintzsche L.E. *et al.*, 2013 *Phys. Rev. B* **88**, 155204
- [27] Anderson N.L, Vedula R.P, and Strachan A, 2015 *Comput. Mater. Science* **109** 124
- [28] DasMahapatra A, and Kroll P, 2018 *Comput. Mater. Science* **148** 165
- [29] Legut D, Wdowik U.D, Kurtyka P, 2014 *Materials Chemistry and Physics* **147**, 42
- [30] Kuzuba T, Kijama K, Bando Y, 1978 *J. Chem. Phys.* **69**, 40
- [31] Xu B *et al.*, 2011 *Phys. Rev. B* **84**, 014113
- [32] Taraskin S N and Elliott S R, 1997 *Phys. Rev. B* **56**, 8605
- [33] Kuwabara A, Matsunaga K, and Tanaka I, 2008 *Phys. Rev. B* **78**, 064104
- [34] Car R and Parrinello M, 1985 *Phys. Rev. Lett.* **55**, 2471
- [35] Pasquarello A, Laasonen K, Car R, Lee CY and Vanderbilt D 1992 *Phys. Rev. Lett.* **69**, 1982 ; Laasonen K, Pasquarello A, Car R, Lee CY and Vanderbilt D 1993 *Phys. Rev. B* **47**, 10142
- [36] Giannozzi P, Baroni S, Bonini N, Calandra M, Car R, Cavazzoni C, Ceresoli D, Chiarotti G

L, Cococcioni M, Dabo I, Dal Corso A, de Gironcoli S, Fabris S, Fratesi G, Gebauer R, Gerstmann R, Gougaussis G, Kokalj A, Lazzari M, Martin-Samos L, Marzari N, Mauri F, Mazzarello R, Paolini S, Pasquarello A, Paulatto L, Sbraccia C, Scandolo S, Sclauzero G, Seitsonen A P, Smogunov A, Umari P, Wentzcovitch R M 2009 *J. Phys.: Condens. Matter* **21** 395502 <http://www.quantum-espresso.org>.

[37] Perdew J P and Zunger A, 1981 *Phys. Rev. B* **23**, 5048

[38] Vanderbilt D, 1990 *Phys. Rev. B* **41**, 7892

[39] Umari P and Pasquarello A, 2002 *Phys. Rev. Lett.* **89**, 157602; I. Souza, J. iguez, and D. Vanderbilt, 2002 *Phys. Rev. Lett.* **89**, 117602

[40] Baroni S, de Gironcoli S, Dal Corso A, Giannozzi P, 2001 *Rev. Mod. Phys.* **73**, 515

[41] Sze S M, *Physics of Semiconductor Devices*, (John Wiley and Sons, Inc. New York 1981).

[42] We used a $2\times 2\times 2$ $\beta\text{-Si}_3\text{N}_4$ supercell that was reshaped from hexagonal to tetragonal without changing the density. Next, we further reshaped the supercell into a cubic one matching the experimental density.

[43] Nosé S, 1984 *Mol. Phys.* **52**, 255; Hoover W G, 1985 *Phys. Rev. A* **31**, 1965

[44] Jarolimek K, de Groot R.A., de Wijs G A, and Zeman M 2010 *Phys. Rev. B* **82**, 205201

[45] Vashishta P, Kalia R K and Ebbsjö I, 1995 *Phys. Rev. Lett.* **75**, 858

[46] Misawa M, Fukunaga T, Niihara K, Hirai T and Suzuki K, 1979 *J. Non-Cryst. Solids* **34**, 313

[47] Mauri A, Celino M, Castellani N, and D. Erbetta, 2011 *Europhys. J* **15**, 02008

[48] Ippolito M and Meloni S, 2011 *Phys. Rev. B* **83**, 165209

[49] Kroll P, 2001 *J. Non-Cryst. Solids* **293-295**, 238

[50] A large nitrogen displacement is clearly not much compatible with the local NSi_3 mode of Fig. 3, and this is reflected by the decrease of the projection above 700 cm^{-1} .

[51] Sarnthein J, Pasquarello A and Car R 1997 *Science* **275**, 1925; Pasquarello A, Sarnthein J and Car R 1998 *Phys. Rev. B* **57**, 14133

[52] Benoit M and Kob W 2002 *Europhys. Lett.* **60**, 269

[53] Loong C -K, Vashishta P, Kalia R K and Ebbsjö I, 1995 *Europhys. Lett.* **31**, 201

[54] Omelchenko A, Nakano A, Kalia R K and Vashishta P, 1996 *Europhys. Lett.* **33**, 667

[55] Jensen J. O. , 2002 *J. Mol. Structure* **588**, 175 ; Miller F A, Perkins J, Gibbon G A, and Swisselm B A, 1974 *J. Raman Spectrosc.* **2**, 93